nature genetics

Haploinsufficiency of MeCP2-interacting transcriptional co-repressor *SIN3A* causes mild intellectual disability by affecting the development of cortical integrity

Josefine S Witteveen[1,13], Marjolein H Willemsen[2,13], Thaís C D Dombroski[1,13], Nick H M van Bakel[1], Willy M Nillesen[2], Josephus A van Hulten[1], Eric J R Jansen[1], Dave Verkaik[2], Hermine E Veenstra-Knol[3], Conny M A van Ravenswaaij-Arts[3], Jolien S Klein Wassink-Ruiter[3], Marie Vincent[4], Albert David[4], Cedric Le Caignec[4,5], Jolanda Schieving[6], Christian Gilissen[2], Nicola Foulds[7,8], Patrick Rump[3], Tim Strom[9,10], Kirsten Cremer[11], Alexander M Zink[11], Hartmut Engels[11], Sonja A de Munnik[2], Jasper E Visser[1,6,12], Han G Brunner[2], Gerard J M Martens[1], Rolph Pfundt[2], Tjitske Kleefstra[2,14] & Sharon M Kolk[1,14]

Numerous genes are associated with neurodevelopmental disorders such as intellectual disability and autism spectrum disorder (ASD), but their dysfunction is often poorly characterized. Here we identified dominant mutations in the gene encoding the transcriptional repressor and MeCP2 interactor switch-insensitive 3 family member A (SIN3A; chromosome 15q24.2) in individuals who, in addition to mild intellectual disability and ASD, share striking features, including facial dysmorphisms, microcephaly and short stature. This phenotype is highly related to that of individuals with atypical 15q24 microdeletions, linking *SIN3A* to this microdeletion syndrome. Brain magnetic resonance imaging showed subtle abnormalities, including corpus callosum hypoplasia and ventriculomegaly. Intriguingly, *in vivo* functional knockdown of *Sin3a* led to reduced cortical neurogenesis, altered neuronal identity and aberrant corticocortical projections in the developing mouse brain. Together, our data establish that haploinsufficiency of *SIN3A* is associated with mild syndromic intellectual disability and that SIN3A can be considered to be a key transcriptional regulator of cortical brain development.

Rapid advances in technologies to identify genetic causes of neurodevelopmental disorders, including intellectual disability, developmental delay and ASD, have led to the identification of numerous copy number variants (CNVs) and dominant gene mutations[1–7]. However, the consequences of the associated protein disturbances mostly remain to be defined. The gene encoding the switch-insensitive 3 transcription regulator family member A (*SIN3A*) is one of five genes located in the shortest region of overlap (SRO; ~260 kb) of 15q24 microdeletions flanked by segmental duplication blocks C and D in individuals with intellectual disability and ASD[8–10]. We now report dominant loss-of-function mutations in *SIN3A* in nine individuals with intellectual disability and developmental delay and hypothesize that haploinsufficiency of *SIN3A* contributes substantially to the phenotype seen in individuals with these deletions. Brain magnetic resonance imaging (MRI) performed in a subset of the individuals showed persistent abnormalities, such as corpus callosum hypoplasia and dysgenesis, and ventriculomegaly.

The development of dedicated cortical brain areas is a highly orchestrated process that involves the proliferation of progenitors, the migration of young neurons to final cortical layers, neuronal differentiation and network formation. Molecular control of cortical progenitor proliferation is directly linked to the eventual size of cortical areas and overall cerebral cortex functioning[11,12]. Furthermore, various intrinsic factors (for example, transcriptional regulators) as well as extrinsic factors (for example, guidance cues) are expressed during the early phases of corticogenesis[13–16], yet the precise roles of many of these factors remain to be elucidated.

In mice, Sin3a can bind to various members of a transcriptional regulatory complex (for example, MeCP2, Hdac1, Hdac2, Ncor and Cabin1) to control a variety of developmental processes[17–21].

[1]Department of Molecular Animal Physiology, Donders Institute for Brain, Cognition and Behavior, Radboud University, Nijmegen, the Netherlands. [2]Department of Human Genetics, Radboud University Medical Center, Donders Institute for Brain, Cognition and Behavior, Nijmegen, the Netherlands. [3]Department of Genetics, University of Groningen, University Medical Center Groningen, Groningen, the Netherlands. [4]Centre Hospitalier Universitaire de Nantes, Service de Génétique Médicale, Nantes, France. [5]Laboratoire de Physiopathologie de la Résorption Osseuse et Thérapie des Tumeurs Osseuses Primitives, Faculté de Médecine, INSERM UMRS 957, Nantes, France. [6]Department of Neurology, Donders Institute for Brain, Cognition and Behavior, Radboud University Medical Center, Nijmegen, the Netherlands. [7]Wessex Clinical Genetics Services, University Hospital Southampton National Health Service Foundation Trust, Princess Anne Hospital, Southampton, UK. [8]Department of Human Genetics and Genomic Medicine, Faculty of Medicine, University of Southampton, Southampton, UK. [9]Institute of Human Genetics, Helmholtz Zentrum München, Neuherberg, Germany. [10]Institute of Human Genetics, Technische Universität München, Munich, Germany. [11]Institute of Human Genetics, University of Bonn, Bonn, Germany. [12]Department of Neurology, Amphia Hospital Breda, Berda, the Netherlands. [13]These authors contributed equally to this work. [14]These authors jointly directed this work. Correspondence should be addressed to S.M.K. (s.kolk@ncmls.ru.nl) or T.K. (tjitske.kleefstra@radboudumc.nl).

Received 11 September 2015; accepted 15 June 2016; published online 11 July 2016; doi:10.1038/ng.3619

Sin3a seems to have an especially important role in cell cycle events and the proliferation of embryonic stem cells[17,19,22–24]. Although Sin3a has been known for over a decade to be present in the rodent forebrain[25–28], its exact role in brain developmental processes remains elusive.

In this report, we investigated the consequences of *SIN3A* haploinsufficiency by comparing clinical and MRI data for nine individuals with intellectual disability and developmental delay in whom we identified *SIN3A* mutations and four so far unpublished cases with *de novo* atypical small 15q24 deletions (breakpoints outside segmental duplication blocks C and D) encompassing *SIN3A* (270–500 kb; SRO 75.60–75.95 Mb, hg19). Furthermore, to investigate the consequences of reduced *Sin3a* expression in brain development, we employed a select *in vivo* functional knockdown assay[29] and found Sin3a to be a key regulator of cortical expansion and maturation. Overall, the observed human syndrome characterized by intellectual disability and developmental delay seems to be a direct consequence of *SIN3A* downregulation by haploinsufficiency affecting correct cortical expansion.

RESULTS

Haploinsufficiency of *SIN3A* causes a distinct syndrome

To better comprehend the consequences of absence of one copy of *SIN3A* or *SIN3A* intragenic loss of function in human brain development, we collected data on the clinical features of four individuals with small deletions in the chromosomal region 15q24 overlapping the *SIN3A* gene (individuals 1–4) and nine individuals with loss-of-function *SIN3A* mutations (individuals 5–13). The clinical features of the individuals with microdeletions and the individuals with dominant mutations were similar and could be classified as a syndrome characterized by mild intellectual disability (defined by total IQ (TIQ) of 50–69), a recognizable facial gestalt and, in some individuals, abnormalities in brain MRI scans, including ventricular dilatation (colpocephaly), corpus callosum dysgenesis and subtle signs of aberrant cortical development (**Fig. 1** and **Table 1**; further clinical descriptions are provided in the **Supplementary Note**). In addition, a subset of individuals with microdeletions or frameshift mutations displayed ASD, hypermobile joints, seizures, microcephaly and short stature (**Table 1** and **Supplementary Note**).

The deletions in individuals 1–4 presented here were detected by genome-wide chromosomal array analysis using different platforms (Online Methods). They all overlap with the previously defined SRO of around 200 kb and encompass five genes, including *SIN3A*. To our knowledge, none of these genes has previously been associated with human disease. The deleted regions of individuals 1–4 and of two previously reported individuals with 15q24 deletions between segmental duplications C and D[9] are shown schematically in **Supplementary Figure 1**. The *SIN3A* intragenic mutations were loss-of-function mutations, including c.803dup (p.Leu269Thrfs*37; individual 5), c.1010_1013del (p.Lys337Serfs*16; individual 6), c.1759_1759delT (p.Ser587Profs*12; individuals 7–9), c.2955_2956delCT (p.Glu985Aspfs*29; individual 10) and c.3310C>T

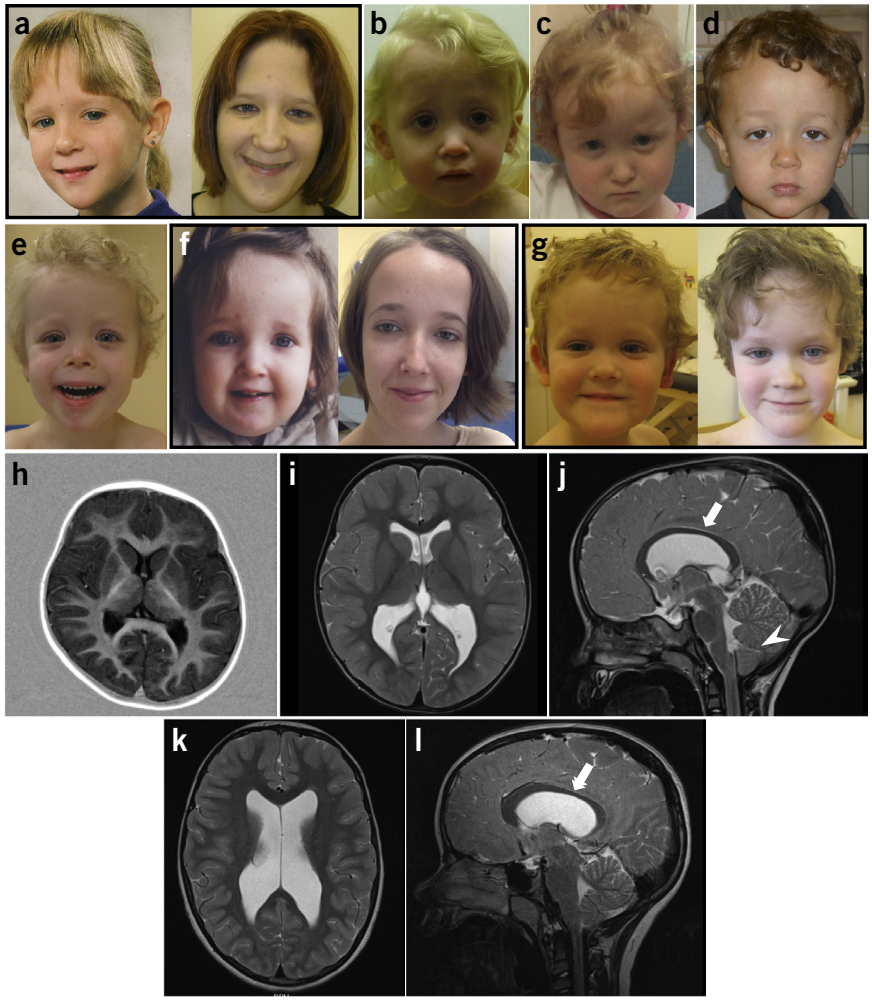

Figure 1 Haploinsufficiency of *SIN3A* causes a distinct syndrome. (**a**–**g**) Clinical photographs of individuals 1–4 with a 15q24 microdeletion and individuals 5, 6 and 10 with a frameshift mutation in *SIN3A*. (**a**) Individual 1 (at 7 years (left) and 26 years (right)). (**b**) Individual 2 (at 2 years). (**c**) Individual 3 (at 4 years). (**d**) Individual 4 (at 3 years and 8 months). (**e**) Individual 5 (at 3 years). (**f**) Individual 6 (at 2 years (left) and 13 years (right)). (**g**) Individual 10 (at 4 years and 7 months (left) and 8 years (right)). Note the overlap in facial appearance, including a broad and high forehead (in all), full eyelids (individuals 2, 4–6 and 10), depressed nose bridge in younger individuals, mildly downslanted palpebral fissures (individuals 1, 2 and 4–6), a pointed or prominent chin (in all), and a small mouth (individuals 3 and 4). Later, facial phenotypes evolved into longer faces (individuals 1 and 6). (**h**–**l**) Brain MRI scans of individuals 1, 5 and 10. (**h**) Transversal short-TI inversion recovery (STIR) MRI scan of individual 1 (at 25 years) showing seemingly underdeveloped frontal lobes (quality is suboptimal). The cortex seems to consist of several small gyri without clear delineation between white and gray matter. Myelination is delayed. (**i**,**j**) Transversal and sagittal MRI scans of individual 5 (at 3 years). (**i**) Ventricles are enlarged (ventriculomegaly), and white matter volume is decreased. (**j**) The scan shows a thin corpus callosum (arrow) and enlarged cerebellar tonsils (arrowhead). (**k**,**l**) Transversal and sagittal MRI scans of individual 10 (at 10 years). (**k**) Ventriculomegaly. (**l**) Hypoplasia of the splenium of the corpus callosum (arrow). Written informed consent was obtained to publish photographs for all individuals shown.

Table 1 Clinical features of six patients with 15q24 microdeletions comprising *SIN3A* and nine patients with a loss-of-function mutation in *SIN3A*

	New 15q24 deletion cases[a]				New loss-of-function mutation cases[b]					Previous deletion cases[a] (Mefford *et al.*[9])		Total
Patient	1	2	3	4	5	6	7–9	10	11–13	14	15	15
Genetic defect	Del 75.60–76.10	Del 75.60–76.10	Del 75.60–76.02	Del 75.60–75.95	c.803dup; p.Leu 269fs	c.1010_1013del; p.Lys337 Serfs	c.1759_1759delT; p.Ser 587fs	c.2955_2956del; p.Glu 985fs	c.3310C>T; p.Arg1104*	Del 75.53–75.80	Del 75.59–76.09	6 deletions, 9 mutations
Inheritance	DN	DN	DN	DN	DN	DN	Inherited	DN	Inherited	DN	DN	2 familial mutations
Sex	F	F	F	M	M	F	2 M, 1 F	M	2 M, 1 F	?	F	7 F, 7 M, 1?
Age at last clinical examination	29 years	4 years, 9 months	4 years	3 years, 8 months	7 years	14 years	16 years, 3 months (index)	9 years, 5 months	4 years, 9 months (index)	20 years	9 years, 5 months	4–45 years
ID (TIQ <70)	+	+	+	+	+	+	+ (index), + (sister), ± (father)	+	+ (index), + brother, ± (mother)	+	–	12/15
Head circumference percentile	P0.6–P2	P3	P10	P25	P16	P75	<P3 (index), NR (sister), P50 (father)	P50	P3 (index), <P0.6 (brother), NR (mother)	P3	P10–P15	6/13 ≤P3
Height percentile	P2	P25	P5	P16	<P0.6	P50	<P3 (index), NR (sister), P50 (father)	P50–75	<P0.6 (index), P2 (brother), <P0.6 (mother)	P50–P75	P3	7/14 ≤P3
Abnormal brain MRI	CD, CC, WM	C, CC, WM	NP	NP	CD, WM, VD	VD	NP (index, father), NR (sister)	CC, VD	NP (index), CD (brother), NR (mother)	NR	CC, VD	7/12
ASD	+	–	–	–	+	+	– (index), NR (sister, father)	+	NR (index), + (brother), NR (mother)	–	+	6/11
Epilepsy	–	+	–	–	+	+	– (index, father), NR (sister)	–	–	NR	NR	3/12
Skeletal abnormalities	NR	–	H	–	H	H	D (index), NR (sister, father)	H	Clinidactyly (index, brother), NR (mother)	H	D	9/10
Hearing loss	+	–	–	–	+	+	– (index), + (sister), – (father)	–	–	NR	NR	4/13
Typical facial dysmorphic features	+	+	+	+	+	+	+ (all)	+	+ (all)	+	+	15/15
Ectodermal symptoms	–	TH	TH	–	TH, N, T	–	NR (all)	–	–	NR	NR	3/9

DN, *de novo*; DD, developmental delay; ID, intellectual disability; NR, not reported; NP, not performed; P, percentile; +, mild ID; ±, low-normal IQ; CD, cortical dysgenesis; CC, corpus callosum dysgenesis; WM, white matter abnormalities; VD, ventricle dilatation; H, hypermobile joints; D, delayed bone age; TH, thin hair; N, brittle nails T, teeth anomalies. [a]The positions (in Mb) of the breakpoints of the deleted regions on chromosome 15 are indicated (UCSC Genome Browser, version hg19). [b]Positions of *SIN3A* mutations are given with respect to NM_001145357.1.

(p.Arg1104*; individuals 11–13), most likely leading to nonsense-mediated decay of the mRNA product and haploinsufficency.

Cortical progenitors and newborn neurons express Sin3a

Sin3a has previously been reported to be involved in various cellular processes[17,19,30] that could contribute to the neurological clinical symptoms observed when it is defective. To first investigate the mRNA and protein expression patterns of SIN3A specifically in the developing human brain, we analyzed expression using the BrainSpan Atlas of the Developing Human Brain (Allen Institute for Brain Science)[31] and of Sin3a in developing mouse brain from embryonic day (E) 10.5 into adulthood (postnatal day (P) 140) employing real-time qPCR and immunohistochemistry. Transcriptome and laser microdissection (LMD) microarray analyses showed the presence of human *SIN3A* mRNA prenatally, with the highest levels in the ventricular zone of various cortical regions, the place where progenitor proliferation occurs (**Supplementary Fig. 2**). Real-time qPCR analysis of developing mouse brain from E10.5 into adulthood (P140) showed that *Sin3a* mRNA is expressed at relatively high levels throughout brain development, with a slight decrease in expression from E16.5–P14 (**Fig. 2a**). Additionally, we analyzed expression of *Sin3a* during development by qPCR in two cortical regions (the prefrontal cortex and somatosensory cortex) at different developmental stages (E16.5–P60), and we found relatively high *Sin3a* expression levels that decreased (E16.5–P14, prefrontal cortex; E16.5–P7, somatosensory cortex) and subsequently increased (P14–adult, prefrontal cortex; P7–adult, somatosensory cortex) over time (**Fig. 2c**). To obtain better spatial resolution for *Sin3a* mRNA expression, we analyzed *in situ* hybridization patterns in adult mouse brain[32–35] (**Fig. 2b**). *Sin3a* was expressed moderately throughout the brain, with somewhat higher expression

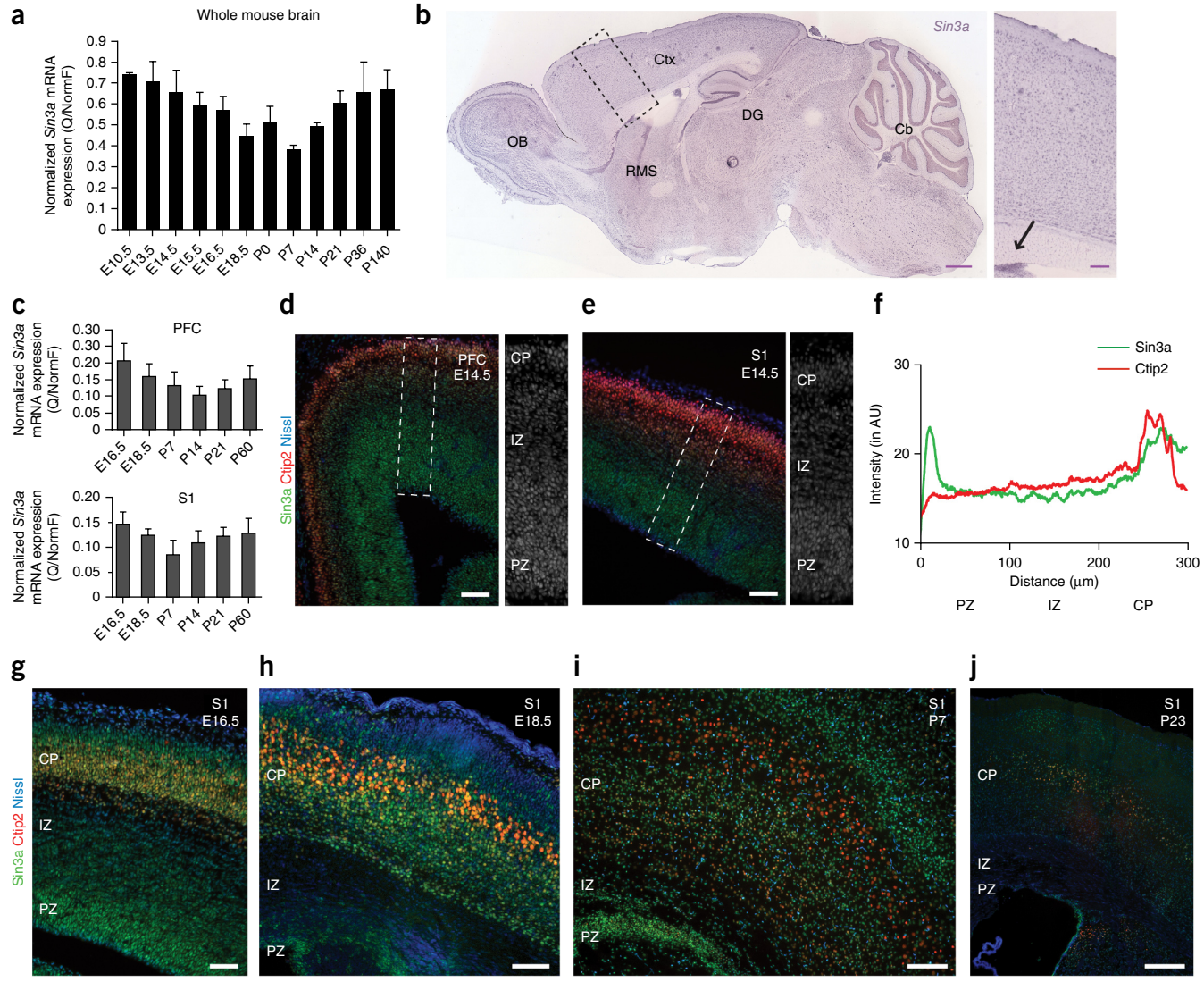

Figure 2 Sin3a is expressed by cortical progenitors. (**a**) *Sin3a* mRNA levels in developing mouse brain from E10.5 and E13.5 heads and E14.5, E15.5, E16.5, E18.5, P0, P7, P14, P21 and adult brain ($n = 3$ series of unrelated mice), as measured by qPCR. Data are presented as normalized mean transcript levels (Q/NormF, qPCR data normalized via normalization factor) ± s.e.m. (**b**) *In situ* hybridization with antisense *Sin3a* (sagittal section of adult mouse brain). *Sin3a* is expressed in neurogenic regions of the subventricular zone (SVZ; arrow in enlargement on the right), rostral migratory stream (RMS), olfactory bulb (OB) and dentate gyrus (DG) of the hippocampus. Scale bars, 300 μm (left) and 50 μm (right). Ctx, cortex; Cb, cerebellum. (**c**) *Sin3a* mRNA levels in developing prefrontal cortex (PFC) and primary somatosensory cortex (S1) in E16.5, E18.5, P7, P14, P21 and adult brain ($n = 3$ series of unrelated mice), as measured by qPCR. Data are presented as normalized mean transcript levels ± s.e.m. (**d**,**e**) Immunostaining for Sin3a (green) and Ctip2 (red) in prefrontal cortex (**d**) and somatosensory cortex (**e**) from E14.5 embryos; sections were counterstained with fluorescent Nissl (blue). An enlargement of the boxed area to the right shows Sin3a staining in gray. CP, cortical plate; IZ, intermediate zone; PZ, proliferative zone. Scale bars, 50 μm. (**f**) Quantification of Sin3a staining (in arbitrary units, AU) in the somatosensory cortex of E14.5 brains from three different mice. (**g**–**j**) Immunostaining for Sin3a (green) and Ctip2 (red) with counterstaining with fluorescent Nissl (blue) in the somatosensory cortex from E16.5 (**g**), E18.5 (**h**), P7 (**i**) and P23 (**j**) brains. Scale bars, 100 μm (**g** and **h**), 50 μm (**i**) and 200 μm (**j**).

in neurogenic regions such as the subventricular zone (**Fig. 2b**), rostral migratory stream, olfactory bulb and dentate gyrus. Within the primary somatosensory cortex, expression was visible in virtually all neurons, with low to moderate expression levels (**Fig. 2b**).

Using a specific antibody against Sin3a, we examined Sin3a protein expression in the developing mouse cerebral cortex during embryogenesis (E14.5–E18.5) and postnatal development (P7–P23). Sin3a was found in various brain regions but was especially apparent in cortical regions such as the prefrontal cortex and somatosensory cortex (**Fig. 2d**,**e**). Sin3a was localized to the nucleus in apical progenitors in the proliferative zone (including the ventricular zone as well as the subventricular zone) and newborn neurons in the intermediate zone and cortical plate, partially colocalizing with the layer 5 marker Ctip2 (**Fig. 2d**–**j** and **Supplementary Fig. 3a**). Although the intensity of Sin3a immunoreactivity in the somatosensory cortex decreased during development, virtually all cells in the cerebral wall were positive, albeit with a high degree of cellular heterogeneity (**Fig. 2f**–**j** and **Supplementary Fig. 3a**). Still, the highest level of Sin3a was detected in the proliferative zone, with fainter staining present in the intermediate zone and moderate staining in the cortical plate (**Fig. 2g**–**j**). Furthermore, Sin3a was present in actively dividing cells in the proliferative zone, as shown by colocalization with the proliferation marker Ki-67 (**Supplementary Fig. 3b**).

Thus, Sin3a is expressed in a large population of cortical progenitors and young neurons during corticogenesis. These expression patterns become more restricted over time, suggestive of expression during the neurogenic phase.

Reduced *Sin3a* leads to decrease in cortical progenitors

Initially, there is lateral cortical expansion within the ventricular zone as neuroepithelial progenitors (radial glial cells) divide symmetrically, with their offspring going into another round of division[36,37]. As development proceeds, cell cycles get longer and radial expansion starts by asymmetric division of subventricular zone progenitors, generating both intermediate progenitors and postmitotic neurons[11,37,38]. Both Sin3a expression patterns and the neurological indications of individuals with a *SIN3A* microdeletion or mutation (dilated ventricles and colpocephaly) hinted at a role for Sin3a in neurogenesis. To determine the potential role of Sin3a in early corticogenesis, we employed a loss-of-function approach. Toward this end, we used two different small hairpin RNA (shRNA) constructs targeting either exon 13 or exon 16 of mouse *Sin3a* mRNA in an *in vivo* knockdown setup. The constructs were introduced by *in utero* electroporation at E14.5, and embryos were euthanized at E17.5 (**Fig. 3b**). First, to validate the effectiveness of *Sin3a* knockdown, we used two small interfering RNAs (siRNAs) targeting exon 13 and exon 16 of *Sin3a* mRNA in a mouse neuroblastoma cell line (N2a). Real-time qPCR, using two primer pairs, showed that endogenous levels of *Sin3a* were comparable between N2a cells and mouse P35 brain, indicating a sufficiently high level of expression to allow knockdown by siRNA transfection (**Supplementary Fig. 4a**). qPCR analysis, using two primer pairs, showed that *Sin3a* transcript levels were considerably decreased 48 h after transfection with the *Sin3a* siRNAs in N2a cells (**Supplementary Fig. 4b**).

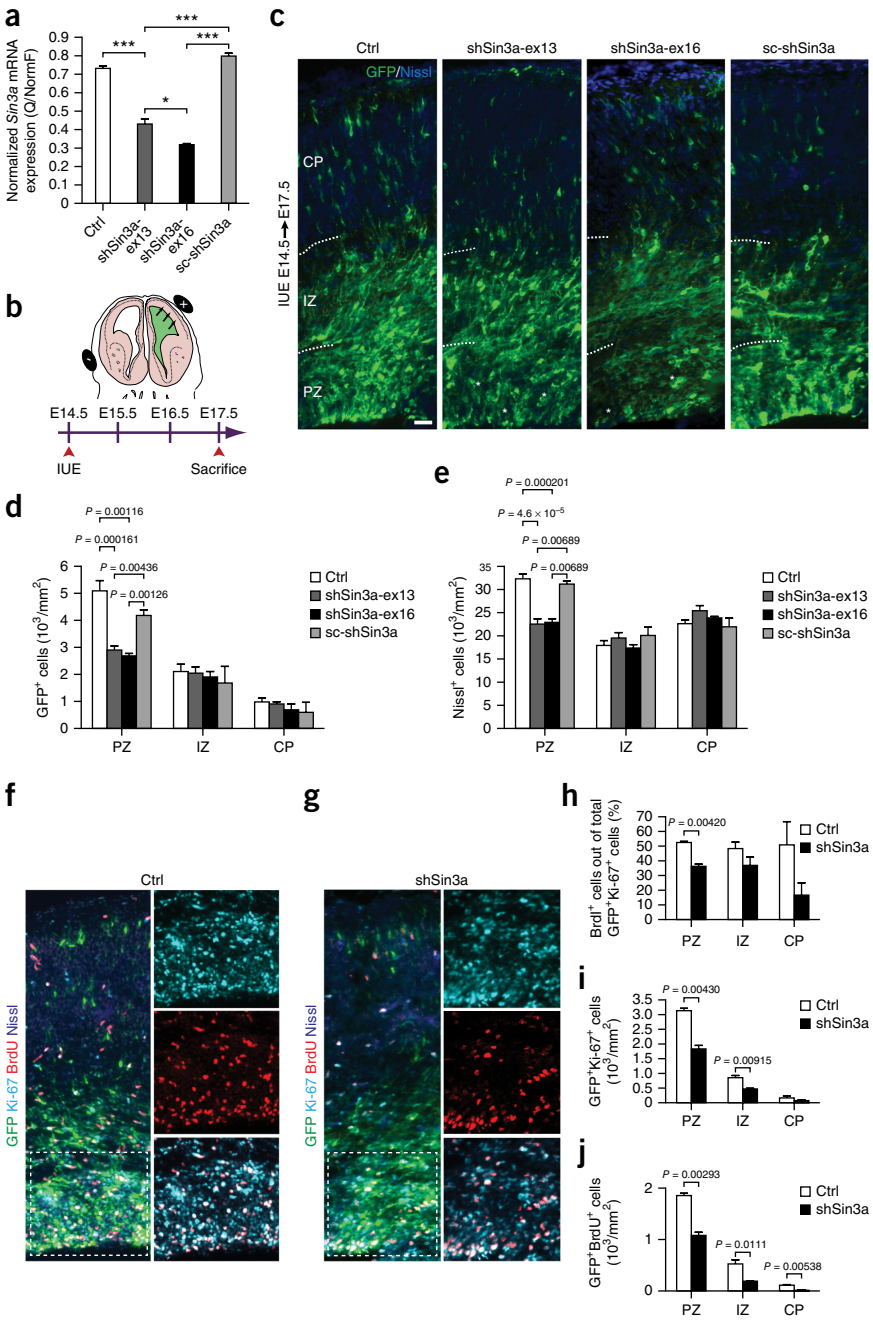

Figure 3 *Sin3a* downregulation decreases the number of cortical progenitors. (**a**) Normalized *Sin3a* mRNA levels in N2a cells transfected with shRNAs targeting *Sin3a* mRNA (shSin3a-ex13 and shSin3a-ex16), a scrambled shRNA (sc-shSin3a) or a control construct expressing GFP (Ctrl). Data are presented as normalized mean transcript levels ± s.e.m. ($n = 3$ biological replicates). Significance was determined by Student's t test (in duplicate with two distinct primer pairs): $^*P < 0.05$, $^{***}P < 0.001$. (**b**) Schematic of *Sin3a* downregulation via *in utero* electroporation (IUE) in cortical regions at E14.5 with embryos sacrificed 3 d later (adapted from ref. 29). (**c**) Mouse cortex electroporated with control construct, scrambled shRNA or *Sin3a* shRNAs at E14.5 and analyzed at E17.5. Sections were immunostained for GFP (green) and counterstained with fluorescent Nissl (blue). Asterisks indicate cell scarcity in the proliferative zone of *Sin3a*-downregulated cortex. Scale bar, 50 µm. (**d**,**e**) Quantification of GFP$^+$ (**d**) and Nissl$^+$ (**e**) cells in the cortical zones (width of 150 µm); $n = 7$ for Ctrl, $n = 7$ for shSin3a-ex13, $n = 4$ for shSin3a-ex16 and $n = 2$ for sc-shSin3a. Data are presented as the number of cells per mm^2 per embryonic zone ± s.e.m. (**f**,**g**) Cortical swatch as in **c** electroporated with either control (**f**) or *Sin3a* shRNA (shSin3a-ex13) (**g**). Sections were immunostained for GFP (green), BrdU (red) and Ki-67 (cyan) and counterstained with fluorescent Nissl (blue). Proliferative zone areas highlighted by the dashed boxes are enlarged on the right with colocalization shown in white. Scale bars, 50 µm. (**h**) Quantification of GFP$^+$Ki-67$^+$BrdU$^+$ cells (percentage of total cells ± s.e.m.) in cortical zones (width of 150 µm); $n = 2$ for Ctrl and $n = 3$ for *Sin3a* shRNA. (**i**) Quantification of GFP$^+$Ki-67$^+$ cells (number of cells per mm^2 per embryonic zone ± s.e.m.) in cortical zones (width of 150 µm); $n = 2$ for Ctrl and $n = 3$ for *Sin3a* shRNA. (**j**) Quantification of GFP$^+$BrdU$^+$ cells (number of cells per mm^2 per embryonic zone ± s.e.m.) in cortical zones (width of 150 µm); $n = 2$ for Ctrl and $n = 3$ for *Sin3a* shRNA. All statistical tests on cell numbers were performed using one-way ANOVA ($\alpha = 0.05$).

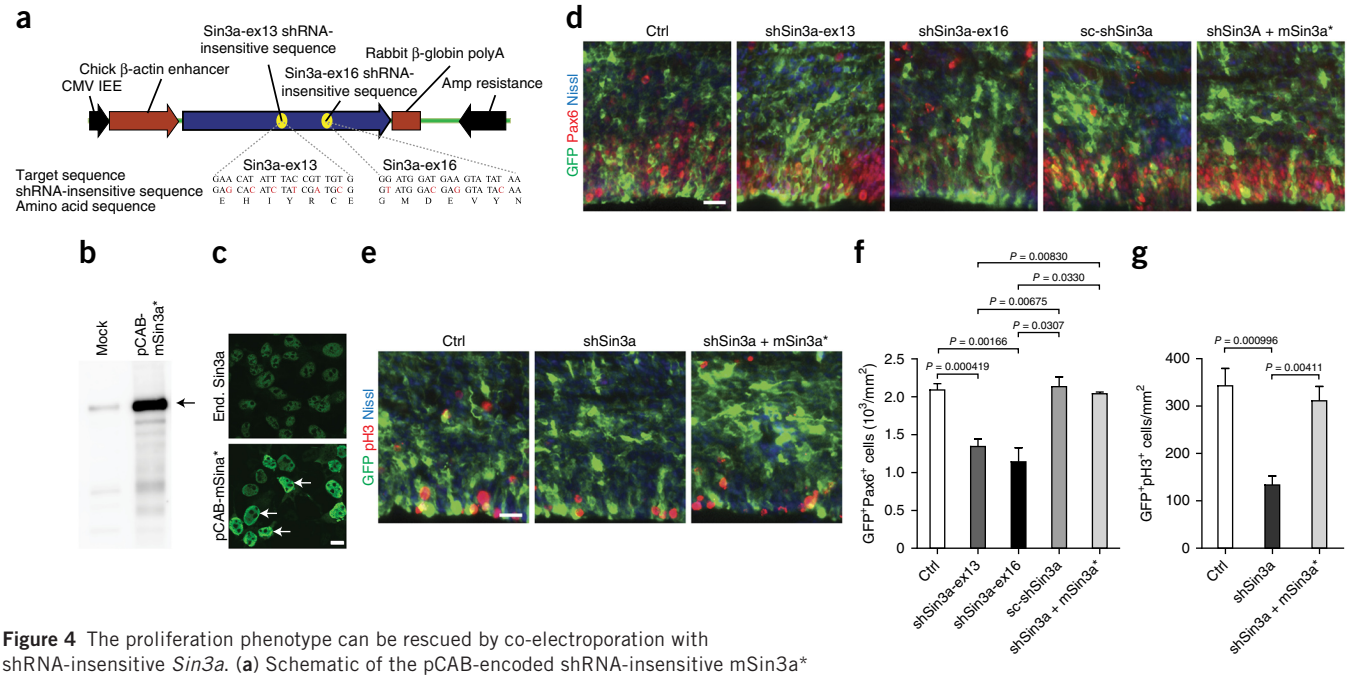

Figure 4 The proliferation phenotype can be rescued by co-electroporation with shRNA-insensitive *Sin3a*. (**a**) Schematic of the pCAB-encoded shRNA-insensitive mSin3a* construct showing site-directed mutagenesis of the two shRNA target areas (yellow). (**b**) Immunoblot showing overexpression of the mSin3a* protein after transfection in COS-1 cells (black arrow). (**c**) COS-1 cells showing endogenous (end.) nuclear Sin3a staining (top) or upregulation of Sin3a expression in the nucleus after expression of mSin3a* (white arrows; bottom). Scale bar, 10 μm. (**d**,**e**) Representative images are shown of the somatosensory cortex proliferative zone electroporated with Ctrl, shSin3a-ex13, shSin3a-ex16, sc-shSin3a, or shRNA for *Sin3a* together with the rescue construct (shSin3a + mSin3a*). Sections were immunostained for GFP (green) together with Pax6 (red) (**d**) or pH3 (red) (**e**). Sections were counterstained with fluorescent Nissl (blue). Scale bars, 50 μm. (**f**) Quantification of the number of GFP$^+$Pax6$^+$ cells in the proliferative zone; $n = 5$ for Ctrl, $n = 5$ for shSin3a-ex13, $n = 3$ for shSin3a-ex16, $n = 2$ for sc-shSin3a and $n = 2$ for shSin3a + mSin3a*. Data are presented as the number of GFP$^+$Pax6$^+$ cells per mm^2 ± s.e.m. One-way ANOVA was used to determine statistical significance ($\alpha = 0.05$). (**g**) Quantification of the number of GFP$^+$pH3$^+$ cells in the proliferative zone; $n = 4$ for Ctrl, $n = 5$ for shSin3a and $n = 2$ for shSin3a + mSin3a*. Data are presented as the number of GFP$^+$pH3$^+$ cells per mm^2 ± s.e.m. One-way ANOVA was used to determine statistical significance ($\alpha = 0.05$).

A reduction in *Sin3a* mRNA levels of about 40% was observed for both siRNA constructs. The sequences of the siRNAs were used to design *Sin3a* shRNAs that were cloned into pSUPER.GFP/Neo vector expressing both the shRNA and GFP (**Supplementary Fig. 4c**). Validation of these constructs by N2a cell transfection followed by measurement of endogenous *Sin3a* mRNA levels by qPCR showed a 50% decrease in *Sin3a* mRNA levels by the shRNA targeting exon 13 and a 60% decrease in *Sin3a* mRNA levels by the shRNA construct targeting exon 16 (**Fig. 3a**).

Next, we electroporated both *Sin3a* shRNA constructs into the developing mouse cortex at E14.5 to study the effect of *Sin3a* down-regulation on cortical development. Three days after electroporation (E17.5), we found that Sin3a protein levels were reduced in the shRNA-electroporated cortices (**Fig. 3b** and **Supplementary Fig. 5a**) and that reduction in Sin3a levels was accompanied by a significant decrease in the proportion of GFP$^+$ cells in the proliferative zone (**Fig. 3c**,**d**). This reduction in cell number was confirmed by Nissl staining, showing significantly lower cell number in *Sin3a*-knockdown embryos than in control embryos (**Fig. 3e** and **Supplementary Fig. 3c**).

The observed decrease in electroporated cell number and total cell number in the proliferative area after reduction of *Sin3a* levels could be caused by a decrease in the number of actively dividing cells. First, to determine whether the decrease in the number of cortical progenitors observed with reduced *Sin3a* levels was due to an increase in cell death, we co-labeled electroporated cells with cleaved caspase 3 (CC3), a marker for caspase-mediated apoptosis. No elevated number of dead cells was observed in either control or *Sin3a*-deficient cortical swatches that were either GFP$^+$ or in the vicinity of GFP$^+$ cells, ruling out autonomous and non-autonomous effects from transfection (**Supplementary Fig. 5b**). We then examined the proliferation state of electroporated progenitors; the results demonstrated a clear decrease in the number of actively dividing cells in the proliferative zone after knockdown of *Sin3a* (**Fig. 3f–h**). To mark all cells in S phase, we administered a BrdU pulse 1.5 h before sacrifice and counted all GFP$^+$Ki-67$^+$BrdU$^+$ cells in the pool of GFP$^+$Ki-67$^+$ cells. Consistent with our earlier observation, GFP$^+$Ki-67$^+$ and GFP$^+$BrdU$^+$ cells in the proliferative zone became sparser when *Sin3a* levels were diminished (**Fig. 3i**,**j**).

Knockdown of *Sin3a* in somatosensory cortex cortical regions resulted in a decrease in neuroprogenitor proliferation. To further assess the role of Sin3a in the generation of cortical neurons and to rescue the observed phenotype, we introduced full-length shRNA-insensitive mouse Sin3a, mSin3a* (**Fig. 4a–c**), and co-labeled the electroporated cortices with Pax6, which labels apical neural stem cells, and phosphorylated histone H3 (pH3), a marker for mitotically active cells. The results showed a clear reduction in the number of GFP$^+$Pax6$^+$ and GFP$^+$pH3$^+$ double-labeled cells after knockdown of *Sin3a*, which was rescued by co-electroporation with the shRNA-insensitive *Sin3a* construct (**Fig. 4d–g**).

Taken together, these results suggest that *Sin3a* causes a decrease in the amount of cortical progenitors in the proliferative zone at the peak of neurogenesis and that Sin3a is essential for early cell division and the production of neurons in the cerebral cortex.

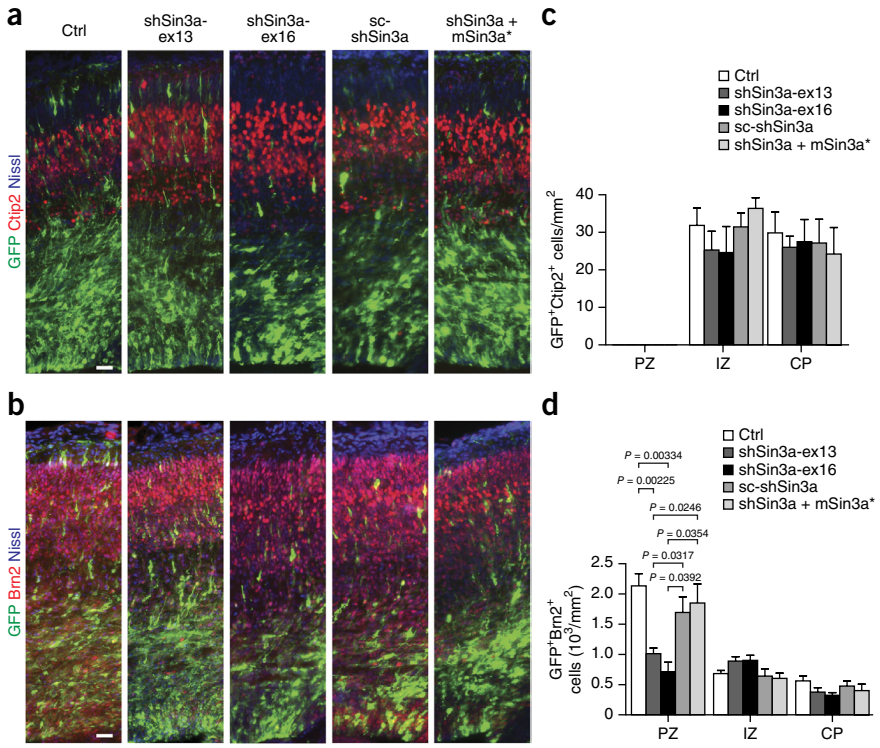

Figure 5 Diminished *Sin3a* levels result in altered layer-specific identity for cortical progenitors. (**a**) Mouse cortexes were electroporated *in utero* at E14.5 with Ctrl, shSin3a-ex13, shSin3a-ex16, sc-shSin3a, or shSin3a + mSin3a* and analyzed at E17.5. Sections were double stained for Ctip2 (red) (**a**) or Brn2 (red) (**b**) and counterstained with fluorescent Nissl (blue). Scale bars, 50 µm. (**c**) Quantification of GFP$^+$Ctip2$^+$ cells in embryonic zones; $n = 4$ for Ctrl, $n = 4$ for shSin3a-ex13, $n = 3$ for shSin3a-ex16, $n = 2$ for sc-shSin3a and $n = 2$ for shSin3a + mSin3a*. Data are presented as the number of GFP$^+$Ctip2$^+$ cells per mm^2 in the embryonic zones ± s.e.m. One-way ANOVA was used to determine statistical significance ($\alpha = 0.05$). (**d**) Quantification of GFP$^+$Brn2$^+$ cells in embryonic zones; $n = 4$ for Ctrl, $n = 4$ for shSin3a-ex13, $n = 3$ for shSin3a-ex16, $n = 2$ for sc-shSin3a and $n = 2$ for shSin3a + mSin3a*. Data are presented as the number of GFP$^+$Brn2$^+$ cells per mm^2 in the embryonic zones ± s.e.m. One-way ANOVA was used to determine statistical significance ($\alpha = 0.05$).

Reduced *Sin3a* results in altered cortical neuronal identity

During development, neuronal progenitors migrate along radial glia cells to the correct cortical layer in an inside-out fashion[39]. Distinct transcription factors mark layer-specific cortical neurons and control their identity[40–42]. To further assess whether the reduction in *Sin3a* levels in cortical proliferative zones had an effect on the migration or identity of cortical progenitors, we performed immunostaining for Ctip2, a layer 5 marker, and Brn2, a marker controlling the identity of neurons in upper layers (layer 2 or 3) (**Fig. 5a**,**b**). At E17.5, the number of GFP$^+$ neurons expressing Ctip2 in the intermediate zone and cortical plate was comparable between cortexes electroporated with

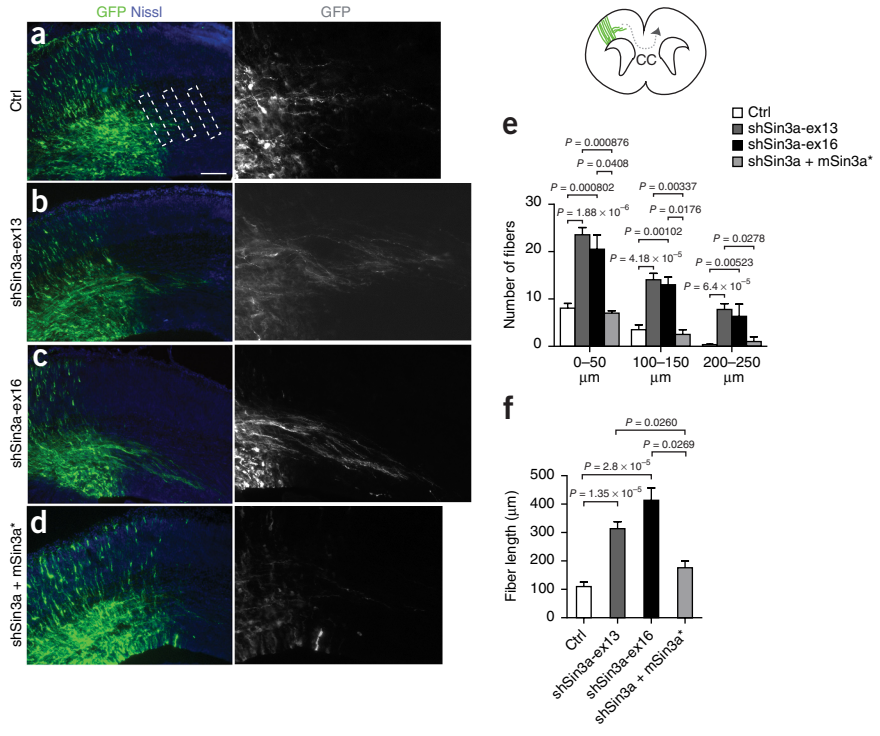

Figure 6 Knockdown of *Sin3a* leads to a neurite outgrowth defect of corticocortical projections. (**a**) A Ctrl-electroporated cortex showing early neurite outgrowth in the intermediate zone. The schematic on the right shows the electroporated area in the somatosensory cortex (green) with the extending neurites and their projection path toward the corpus callosum (CC; gray dotted line). Right, enlargement showing extending neurites. (**b**) An shSin3a-ex13–electroporated cortex showing early neurite outgrowth in the intermediate zone. Right, enlargement showing aberrantly extending neurites. (**c**) An shSin3a-ex16–electroporated cortex showing early neurite outgrowth in the intermediate zone. Right, enlargement showing aberrantly extending neurites. (**d**) A cortex electroporated with shSin3a-ex13 together with the rescue construct mSin3a* showing early neurite outgrowth in the intermediate zone. Right, enlargement showing extending neurites. Scale bars, 100 µm for **a**–**d**. (**e**) Quantification of neurite number in each of the three bins (dashed boxes in **a**; $n = 7$ for Ctrl, $n = 7$ for shSin3a-ex13, $n = 3$ for shSin3a-ex16 and $n = 2$ for shSin3a + mSin3a*). Data are presented as the mean number of extending neurites ± s.e.m. One-way ANOVA was used to determine statistical significance ($\alpha = 0.05$). (**f**) Quantification of the length of the ten longest neurites ($n = 7$ for Ctrl, $n = 7$ for shSin3a-ex13, $n = 3$ for shSin3a-ex16 and $n = 2$ for shSin3a + mSin3a*). Data are presented as the mean length of the ten longest neurites ± s.e.m. One-way ANOVA was used to determine statistical significance ($\alpha = 0.05$).

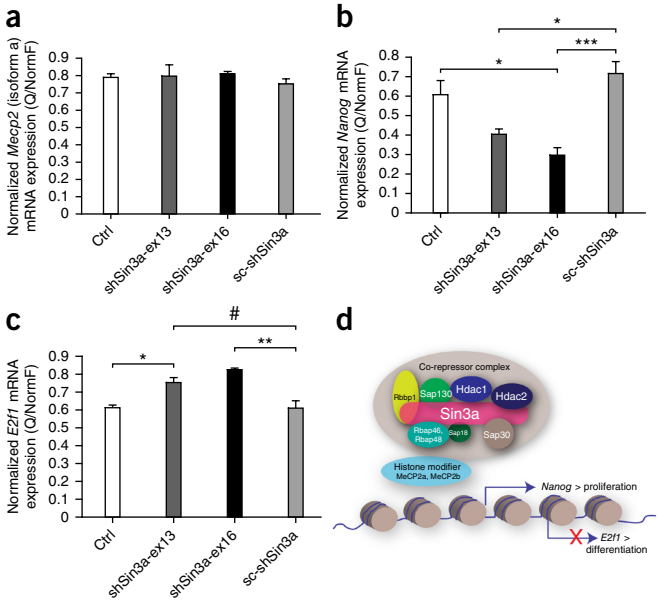

Figure 7 Knockdown of *Sin3a* mRNA in N2a cells by shRNAs affects *Nanog* and *E2f1* expression. (**a**) Normalized mRNA levels for the co-repressor *Mecp2* (isoform a) did not change 48 h after knockdown of *Sin3a* ($n = 3$ biological replicates). (**b**) Normalized mRNA levels of *Nanog* were decreased 48 h after knockdown of *Sin3a* ($n = 3$ biological replicates). (**c**) Normalized mRNA levels of *E2f1* were increased 48 h after knockdown of *Sin3a* ($n = 3$ biological replicates). Data are presented as normalized mean transcript levels ± s.e.m. Student's *t*-test was used to determine significance: $^{\#}0.1 > P > 0.05$, $^{*}P < 0.05$, $^{**}P < 0.01$, $^{***}P < 0.001$. (**d**) Schematic model representing the function of Sin3a in neuronal progenitors.

control and *Sin3a* shRNA (**Fig. 5a**,**c**), although there seemed to be fewer GFP$^+$Ctip2$^+$ cells in the intermediate zone when *Sin3a* was downregulated (**Fig. 5c**). The number of GFP$^+$ cells expressing Brn2, however, was significantly lower in the proliferative zone of cortex electroporated with shRNA for *Sin3a* and seemed to be slightly higher in the intermediate zone (**Fig. 5b**,**d**). The number of GFP$^+$Brn2$^+$ cells was restored to relatively normal levels when shRNA-insensitive *Sin3a* was co-electroporated (**Fig. 5d**). These data suggest that neurons with lower Sin3a levels have changed their identity, which implies that Sin3a is required for differentiation of cortical progenitors.

Sin3a affects cortical differentiation and axon elongation

In their target cortical layers, postmitotic neurons start extending their leading and trailing processes, which become functional dendrites and axons, respectively[43,44]. Trailing processes in the intermediate zone navigate toward the corpus callosum by extension[45]. We assessed the characteristics of electroporated neurons in the cortical plate in terms of their ability to connect to the contralateral cortex by axon elongation when *Sin3a* was downregulated. We first checked at E17.5 whether neuronal polarity (multipolar-to-bipolar transition) was affected. Categorizing the newly generated neurons in the intermediate zone of somatosensory cortex electroporated with either control or *Sin3a* shRNA on the basis of their morphology (multipolar, bipolar or unipolar) and assessing the percentage in each category showed no significant difference (data not shown). However, inspection of callosal axons emerging from transfected neurons demonstrated that downregulation of *Sin3a* increased both the length and number of axons following the callosal path and crossing the midline, with some axons deviating from the original tract (**Fig. 6a**–**f**). These results strongly support a role for Sin3a in cortical neuron differentiation and callosal axon elongation *in vivo*.

Reduced *Sin3a* affects Sin3a partner and target expression

Given the expression of Sin3a in cortical progenitors and the abnormal proliferation and cell fate patterns in *Sin3a*-knockdown mouse cortex, we asked whether knockdown of *Sin3a* in N2a cells would affect expression levels of the well-known Sin3a binding partners MeCP2a and MeCP2b[46,47] or downstream targets of Sin3a that are known to have a role in proliferation or differentiation such as Nanog[19,48,49], cyclin D1 (refs. 17,50), Cdkn1a[51,52] and E2f1 (refs. 53–55). N2a cells were transfected with shRNA targeting *Sin3a* or control constructs for 48 h. We then analyzed transcript levels for isoforms a and b of *Mecp2*, *Nanog*, *Ccnd1*, *Cdkn1a* and *E2f1* by qPCR. Upon downregulation of *Sin3a* (**Fig. 3a**), the expression levels of transcripts for the binding partners in the repressor complex, MeCP2a and MeCP2b, were comparable to control levels (**Fig. 7a** and **Supplementary Fig. 4i**). In contrast to this, we found that expression levels of the target *Nanog* were reduced by 50–60% (**Fig. 7b**), that is, in a similar fashion to *Sin3a*. We found no significant change in transcript levels for *Ccnd1* or *Cdkn1a* (**Supplementary Fig. 4h**,**j**). Of note, knockdown of *Sin3a* significantly derepressed *E2f1* levels by approximately 30% (**Fig. 7c**). These findings suggest that Sin3a is a key member of the complex regulating the expression levels of transcription factors involved in proliferation and differentiation (**Fig. 7d**).

DISCUSSION

In this study, we show that loss of function of *SIN3A* in humans is associated with a distinct intellectual disability and developmental delay syndrome and identify SIN3A as a key factor in corticogenesis. The considerable number of affected individuals allows us to draw firm conclusions relating *SIN3A* variations to clinical symptoms of the syndrome. Together with the complementary data generated by mouse *in utero* electroporation studies, we establish Sin3a as an important regulator of mammalian cerebral cortex development.

SIN3A is added to a number of genes encoding epigenetic factors that are implicated in intellectual disability and ASD[56]. Moreover, SIN3A interacts with various proteins that have already been shown to contribute to intellectual disability phenotypes and display a neuronal function, such as MeCP2, HDAC and MLL proteins[25,57]. Interestingly, one of the best studied and closest interactors of SINA3 is the MeCP2 protein, which is associated with Rett syndrome (MIM 312750)[57,58]. Loss of *Mecp2* in mice causes synaptic defects in neural circuit development by dysregulating GABAergic transmission and cortical excitability[59,60]. This impaired functioning of the cortical circuit is thought to underlie the loss of motor and cognitive abilities and the impaired social interactions seen in individuals with Rett syndrome[60–64].

The phenotype we observed in the individuals with loss-of-function mutations in *SIN3A* is highly similar to the phenotype in individuals with microdeletions in the same chromosomal region, strongly supporting a causal role for haploinsufficiency of *SIN3A* in the reported intellectual disability and developmental delay phenotypes of the individuals with a 15q24 microdeletion between segmental duplication blocks C and D. The level of intellectual disability and developmental delay is in the mild to low-normal range, which explains the presence of inherited changes in two unrelated families with a mildly affected parent and more severely affected children. This finding is in agreement with a recent report on a familial 15q24 deletion encompassing *SIN3A* segregating in twins and their father[65].

Besides intellectual disability and developmental delay, ASD features were present in six individuals. One potential loss-of-function variant in *SIN3A* was found to be present in the Exome Aggregation Consortium (ExAC) population database. However, this variant is classified as 'low confidence', as it was derived from a study with low sequencing coverage. Furthermore, the variant is not located in the coding sequence of any *SIN3A* transcript, and it is therefore likely not of functional relevance.

Other shared clinical features include a marked overlap in facial gestalt, microcephaly, (relatively) small head circumference, (relatively) short stature, hypermobile joints, hearing loss and ectodermal symptoms such as thin hair. In addition to ASD, obsessive–compulsive behaviors and attention and concentration problems were observed in several individuals. We also noticed a history of mild seizures in three individuals. Cerebral imaging (MRI) was performed in eight of the ten indexed individuals. Dilated ventricles, colpocephaly and corpus callosum dysgenesis were the most consistent abnormalities observed. Of note, four individuals showed some irregularities of the cortex (**Fig. 1h–j**), although these abnormalities were subtle and evaluation of the MRI scans was hampered by suboptimal quality. Altogether, the observed human phenotypes prompted us to study the role of SIN3A in brain development.

Mouse Sin3a protein closely resembles its human homolog[66]. *In utero* gene transfer to knock down *Sin3a* in mice produced a clear cortical phenotype with features that resemble the human symptoms. Although there are differences between the human and mouse manifestations, the observed phenotype is reminiscent of disturbances in early cell proliferation. Of note, microcephaly is observed in a large number of the human cases (6/13; 46%), which seems in line with impaired proliferation. The observed enhanced neurite outgrowth in *Sin3a*-knockdown mice can be a cause of premature cell cycle exit for neurons normally migrating toward layer 2 or 3 of the cortical plate. By becoming postmitotic at the wrong time and place, these neurons start to extend their neurites too early, which might be the prerequisite for the longitudinal callosal projections, or Probst bundles, often observed in callosal dysgenesis[45,67].

Over the last few years, genetic studies, fueled by the emergence of whole-exome and whole-genome sequencing, have identified a number of genes involved in cortical malformations[61,63,68,69]. Some of these genes are involved in early proliferation of progenitors, resulting in primary microcephaly and intellectual disability when mutated. For example, mutations in *WDR62* cause severe cortical malformations, including microcephaly, pachygyria with cortical thickening and hypoplasia of the corpus callosum[70]. As a result of spindle instability, cortical progenitors lacking *WDR62* undergo premature differentiation, eventually leading to mitotic arrest and cell death, which underlie the malformations[69,71–73]. Another transcription factor, Tbr1, regulates axonal projections from the amygdala[74] and influences the regional and laminar fate of the developing cortex[75,76]. Next-generation sequencing discovered that *de novo TBR1* mutations cause ASD as well as intellectual disability[74,77–79].

The observed phenotype with *Sin3a* deficiency furthermore raises the possibility that the diminished number of Brn2$^+$ neurons with decreased levels of *Sin3a* is a result of increased differentiation of cortical progenitors. This is in line with the neurite outgrowth results showing premature outgrowth when *Sin3a* levels are downregulated. Increased differentiation would most likely result in aberrant projections, leading to compensatory mechanisms such as pruning of the projections as they are hampered in getting to the correct target area[80]. More experiments using BrdU in a cell cycle exit and cell fate paradigm will shed light on the exact functioning of Sin3a.

As a transcriptional regulator, the SIN3–HDAC–MeCP2 co-repressor complex is involved in diverse functions during various phases of life, including embryonic development[17,30,81]. For example, in embryonic stem cells, expression of *Nanog* is upregulated via the Sin3–Hdac complex and is downregulated during differentiation[17,48,82]. Interestingly, in our studies, reduced *Sin3a* expression in N2a cells led to lower *Nanog* transcript levels. *E2f1*, as a Sin3a downstream target, is inversely correlated with the proliferation rate of cerebellar progenitors and is upregulated postnatally[54], a phenomenon we can clearly correlate with the proliferation rate of cortical progenitors that was diminished following *Sin3a* knockdown. Yet, how these downstream targets relate to the transcription factor Brn2 or any other marker for layer-specific cortical identity needs to be elucidated. Knockdown studies in mice have demonstrated that Sin3a is involved in embryogenesis[22] and synaptic plasticity in the rodent forebrain[25,26]. However, we found for the first time to our knowledge that Sin3a is crucial for the early steps in cortical development, such as proliferation, determination of cell fate and axon outgrowth.

Development of the human cerebral cortex is a tightly orchestrated process that is unique among all vertebrates. The timely events of cortical proliferation, neuronal migration, differentiation, axonal guidance and connectivity are a prerequisite for the higher-order functioning of humans. The clinical observations together with the results of our functional studies in mouse brain demonstrate a crucial role for *SIN3A* in these processes. The present era of high-throughput genome sequencing in combination with brain imaging in intellectual disability, developmental delay and/or ASD alongside preclinical cellular and animal studies will allow us to identify other important players in the development of cortical integrity.

URLs. Allen Institute for Brain Science BrainSpan Atlas of the Developing Human Brain, http://www.brainspan.org/; BrainMap database, http://www.brainmap.org/; Allen Brain Atlas, http://mouse.brain-map.org/; siRNA selection program, http://sirna.wi.mit.edu/; DECIPHER database, https://decipher.sanger.ac.uk/; Radboud Institute for Molecular Life Sciences Microscope Imaging Centre (MIC), http://www.rimls.nl/technology-centers-old/microscope-imaging-centre/; GeNORM program, https://genorm.cmgg.be/.

METHODS

Methods and any associated references are available in the online version of the paper.

Note: Any Supplementary Information and Source Data files are available in the online version of the paper.

ACKNOWLEDGMENTS

We thank laboratory members and colleagues for critically reading this manuscript and members of the various laboratories for helpful editing and discussions. We express thanks to W. Hendriks (Radboud University) for sharing plasmids and N. Nadif Kasri (Radboud University Medical Center) for kindly providing antibody to mouse Ki-67. We are grateful for the mouse *Sin3a* cDNA clone from R. Floyd and B.D. Hendrich (Wellcome Trust Centre for Stem Cell Research and MRC Centre for Stem Cell Biology and Regenerative Medicine). We thank the Radboud Institute for Molecular Life Sciences microscopy platform (see URLs) for excellent support and maintenance of the equipment. We are grateful to the families and subjects participating in this study for their involvement. This work was supported by funding from Science without Borders, CAPES-Brasil (BEX 12044/13-0) to T.C.D.D., complemented by extra support from the Educational Institute of Biosciences at Radboud University, by grants from the Netherlands Organization for Health Research and Development, ZonMw (grant 907-00-365) to T.K., by the Dutch Brain Foundation (HsN F2014(1)-16) to J.E.V. and by the German Ministry of Research and Education (grants 01GS08164, 01GS08167 and 01GS08163 German Mental Retardation Network) to H.E. and T.S., as part of the National Genome Research Network.

AUTHOR CONTRIBUTIONS

The study was designed and directed by T.K. and S.M.K. Patient ascertainment and recruitment were carried out by T.K., M.H.W., H.E.V.-K., C.M.A.v.R.-A., D.V., J.S.K.W.-R., M.V., A.D., J.S., P.R., N.F., K.C., S.A.d.M., C.L.C. and H.G.B. Microarray analyses, DNA sequencing, validation and genotyping were carried out and interpreted by W.M.N., T.S., A.M.Z., H.E. and J.S.W. C.G. was responsible for the bioinformatics of human genetic data analyses. R.P., T.C.D.D., N.H.M.v.B. and E.J.R.J. performed the *in vitro* functional assays, cloning and mouse experiments. J.E.V. interpreted the *in vitro* functional assays, cloning and mouse experiments. J.A.v.H. was invaluable in mouse care. The manuscript was written by J.S.W., M.H.W., T.C.D.D., G.J.M.M., T.K. and S.M.K., with all authors refining and approving the final version of it.

COMPETING FINANCIAL INTERESTS

The authors declare no competing financial interests.

1. Lugtenberg, D. *et al. De novo* loss-of-function mutations in *WAC* cause a recognizable intellectual disability syndrome and learning deficits in *Drosophila*. *Eur. J. Hum. Genet.* http://dx.doi.org/10.1038/ejhg.2015.282 (2016).
2. Willemsen, M.H. & Kleefstra, T. Making headway with genetic diagnostics of intellectual disabilities. *Clin. Genet.* **85**, 101–110 (2014).
3. Willemsen, M.H. *et al.* Chromosome 1p21.3 microdeletions comprising *DPYD* and *MIR137* are associated with intellectual disability. *J. Med. Genet.* **48**, 810–818 (2011).
4. Samocha, K.E. *et al.* A framework for the interpretation of *de novo* mutation in human disease. *Nat. Genet.* **46**, 944–950 (2014).
5. Coe, B.P. *et al.* Refining analyses of copy number variation identifies specific genes associated with developmental delay. *Nat. Genet.* **46**, 1063–1071 (2014).
6. Gilissen, C. *et al.* Genome sequencing identifies major causes of severe intellectual disability. *Nature* **511**, 344–347 (2014).
7. Jansen, S. *et al. De novo* loss-of-function mutations in X-linked *SMC1A* cause severe ID and therapy resistant epilepsy in females: expanding the phenotypic spectrum. *Clin. Genet.* http://dx.doi.org/10.1111/cge.12729 (2016).
8. Magoulas, P.L. & El-Hattab, A.W. Chromosome 15q24 microdeletion syndrome. *Orphanet J. Rare Dis.* **7**, 2 (2012).
9. Mefford, H.C. *et al.* Further clinical and molecular delineation of the 15q24 microdeletion syndrome. *J. Med. Genet.* **49**, 110–118 (2012).
10. Andrieux, J. *et al.* Genotype–phenotype correlation in four 15q24 deleted patients identified by array-CGH. *Am. J. Med. Genet. A.* **149A**, 2813–2819 (2009).
11. Borrell, V. & Reillo, I. Emerging roles of neural stem cells in cerebral cortex development and evolution. *Dev. Neurobiol.* **72**, 955–971 (2012).
12. Fish, J.L., Dehay, C., Kennedy, H. & Huttner, W.B. Making bigger brains—the evolution of neural-progenitor-cell division. *J. Cell Sci.* **121**, 2783–2793 (2008).
13. Laguesse, S., Peyre, E. & Nguyen, L. Progenitor genealogy in the developing cerebral cortex. *Cell Tissue Res.* **359**, 17–32 (2015).
14. Schubert, D., Martens, G.J. & Kolk, S.M. Molecular underpinnings of prefrontal cortex development in rodents provide insights into the etiology of neurodevelopmental disorders. *Mol. Psychiatry* **20**, 795–809 (2015).
15. Bielen, H. & Houart, C. The Wnt cries many: Wnt regulation of neurogenesis through tissue patterning, proliferation, and asymmetric cell division. *Dev. Neurobiol.* **74**, 772–780 (2014).
16. LaMonica, B.E., Lui, J.H., Wang, X. & Kriegstein, A.R. OSVZ progenitors in the human cortex: an updated perspective on neurodevelopmental disease. *Curr. Opin. Neurobiol.* **22**, 747–753 (2012).
17. Dannenberg, J.H. *et al.* mSin3A corepressor regulates diverse transcriptional networks governing normal and neoplastic growth and survival. *Genes Dev.* **19**, 1581–1595 (2005).
18. Gallagher, S.J. *et al.* Distinct requirements for *Sin3a* in perinatal male gonocytes and differentiating spermatogonia. *Dev. Biol.* **373**, 83–94 (2013).
19. McDonel, P., Demmers, J., Tan, D.W., Watt, F. & Hendrich, B.D. Sin3a is essential for the genome integrity and viability of pluripotent cells. *Dev. Biol.* **363**, 62–73 (2012).
20. Gajan, A., Barnes, V.L., Liu, M., Saha, N. & Pile, L.A. The histone demethylase dKDM5/LID interacts with the SIN3 histone deacetylase complex and shares functional similarities with SIN3. *Epigenetics Chromatin* **9**, 4 (2016).
21. Saha, N., Liu, M., Gajan, A. & Pile, L.A. Genome-wide studies reveal novel and distinct biological pathways regulated by SIN3 isoforms. *BMC Genomics* **17**, 111 (2016).
22. Cowley, S.M. *et al.* The mSin3A chromatin-modifying complex is essential for embryogenesis and T-cell development. *Mol. Cell. Biol.* **25**, 6990–7004 (2005).
23. Nascimento, E.M. *et al.* The opposing transcriptional functions of Sin3a and c-Myc are required to maintain tissue homeostasis. *Nat. Cell Biol.* **13**, 1395–1405 (2011).
24. Bansal, N., David, G., Farias, E. & Waxman, S. Emerging roles of epigenetic regulator Sin3 in cancer. *Adv. Cancer Res.* **130**, 113–135 (2016).
25. Schoch, H. & Abel, T. Transcriptional co-repressors and memory storage. *Neuropharmacology* **80**, 53–60 (2014).
26. Kadamb, R., Mittal, S., Bansal, N., Batra, H. & Saluja, D. Sin3: insight into its transcription regulatory functions. *Eur. J. Cell Biol.* **92**, 237–246 (2013).
27. Huang, Y., Myers, S.J. & Dingledine, R. Transcriptional repression by REST: recruitment of Sin3A and histone deacetylase to neuronal genes. *Nat. Neurosci.* **2**, 867–872 (1999).
28. Kyrylenko, S., Korhonen, P., Kyrylenko, O., Roschier, M. & Salminen, A. Expression of transcriptional repressor proteins mSin3A and 3B during aging and replicative senescence. *Biochem. Biophys. Res. Commun.* **275**, 455–459 (2000).
29. Kolk, S.M., de Mooij-Malsen, A.J. & Martens, G.J. Spatiotemporal molecular approach of *in utero* electroporation to functionally decipher endophenotypes in neurodevelopmental disorders. *Front. Mol. Neurosci.* **4**, 37 (2011).
30. Swaminathan, A. & Pile, L.A. Regulation of cell proliferation and wing development by *Drosophila* SIN3 and String. *Mech. Dev.* **127**, 96–106 (2010).
31. Miller, J.A. *et al.* Transcriptional landscape of the prenatal human brain. *Nature* **508**, 199–206 (2014).
32. Lein, E.S. *et al.* Genome-wide atlas of gene expression in the adult mouse brain. *Nature* **445**, 168–176 (2007).
33. Laird, A.R., Lancaster, J.L. & Fox, P.T. BrainMap: the social evolution of a human brain mapping database. *Neuroinformatics* **3**, 65–78 (2005).
34. Fox, P.T. *et al.* BrainMap taxonomy of experimental design: description and evaluation. *Hum. Brain Mapp.* **25**, 185–198 (2005).
35. Fox, P.T. & Lancaster, J.L. Mapping context and content: the BrainMap model. *Nat. Rev. Neurosci.* **3**, 319–321 (2002).
36. Götz, M. & Huttner, W.B. The cell biology of neurogenesis. *Nat. Rev. Mol. Cell Biol.* **6**, 777–788 (2005).
37. Noctor, S.C., Martínez-Cerdeño, V., Ivic, L. & Kriegstein, A.R. Cortical neurons arise in symmetric and asymmetric division zones and migrate through specific phases. *Nat. Neurosci.* **7**, 136–144 (2004).
38. Noctor, S.C., Martínez-Cerdeño, V. & Kriegstein, A.R. Distinct behaviors of neural stem and progenitor cells underlie cortical neurogenesis. *J. Comp. Neurol.* **508**, 28–44 (2008).
39. Evsyukova, I., Plestant, C. & Anton, E.S. Integrative mechanisms of oriented neuronal migration in the developing brain. *Annu. Rev. Cell Dev. Biol.* **29**, 299–353 (2013).
40. Molyneaux, B.J., Arlotta, P., Menezes, J.R. & Macklis, J.D. Neuronal subtype specification in the cerebral cortex. *Nat. Rev. Neurosci.* **8**, 427–437 (2007).
41. Leone, D.P., Srinivasan, K., Chen, B., Alcamo, E. & McConnell, S.K. The determination of projection neuron identity in the developing cerebral cortex. *Curr. Opin. Neurobiol.* **18**, 28–35 (2008).
42. Shoemaker, L.D. & Arlotta, P. Untangling the cortex: advances in understanding specification and differentiation of corticospinal motor neurons. *BioEssays* **32**, 197–206 (2010).
43. Namba, T. *et al.* Pioneering axons regulate neuronal polarization in the developing cerebral cortex. *Neuron* **81**, 814–829 (2014).
44. Zolessi, F.R., Poggi, L., Wilkinson, C.J., Chien, C.B. & Harris, W.A. Polarization and orientation of retinal ganglion cells *in vivo*. *Neural Dev.* **1**, 2 (2006).
45. Hatanaka, Y. *et al.* Distinct roles of neuropilin 1 signaling for radial and tangential extension of callosal axons. *J. Comp. Neurol.* **514**, 215–225 (2009).
46. Nan, X. *et al.* Transcriptional repression by the methyl-CpG-binding protein MeCP2 involves a histone deacetylase complex. *Nature* **393**, 386–389 (1998).
47. Boeke, J., Ammerpohl, O., Kegel, S., Moehren, U. & Renkawitz, R. The minimal repression domain of MBD2b overlaps with the methyl-CpG-binding domain and binds directly to Sin3A. *J. Biol. Chem.* **275**, 34963–34967 (2000).
48. Baltus, G.A., Kowalski, M.P., Tutter, A.V. & Kadam, S. A positive regulatory role for the mSin3A–HDAC complex in pluripotency through Nanog and Sox2. *J. Biol. Chem.* **284**, 6998–7006 (2009).
49. Liang, J. *et al.* Nanog and Oct4 associate with unique transcriptional repression complexes in embryonic stem cells. *Nat. Cell Biol.* **10**, 731–739 (2008).
50. Rampalli, S., Pavithra, L., Bhatt, A., Kundu, T.K. & Chattopadhyay, S. Tumor suppressor SMAR1 mediates cyclin D1 repression by recruitment of the SIN3/histone deacetylase 1 complex. *Mol. Cell. Biol.* **25**, 8415–8429 (2005).
51. Ji, Q. *et al.* CRL4B interacts with and coordinates the SIN3A–HDAC complex to repress *CDKN1A* and drive cell cycle progression. *J. Cell Sci.* **127**, 4679–4691 (2014).
52. Pollock, A., Bian, S., Zhang, C., Chen, Z. & Sun, T. Growth of the developing cerebral cortex is controlled by microRNA-7 through the p53 pathway. *Cell Reports* **7**, 1184–1196 (2014).
53. van Oevelen, C. *et al.* A role for mammalian Sin3 in permanent gene silencing. *Mol. Cell* **32**, 359–370 (2008).
54. Suzuki, D.E., Ariza, C.B., Porcionatto, M.A. & Okamoto, O.K. Upregulation of E2F1 in cerebellar neuroprogenitor cells and cell cycle arrest during postnatal brain development. *In Vitro Cell. Dev. Biol. Anim.* **47**, 492–499 (2011).
55. Kim, Y. *et al.* Activation of Cdk2–pRB–E2F1 cell cycle pathway by repeated electroconvulsive shock in the rat frontal cortex. *Biol. Psychiatry* **57**, 107–109 (2005).
56. Kleefstra, T., Schenck, A., Kramer, J.M. & van Bokhoven, H. The genetics of cognitive epigenetics. *Neuropharmacology* **80**, 83–94 (2014).
57. Chahrour, M. & Zoghbi, H.Y. The story of Rett syndrome: from clinic to neurobiology. *Neuron* **56**, 422–437 (2007).
58. Damen, D. & Heumann, R. MeCP2 phosphorylation in the brain: from transcription to behavior. *Biol. Chem.* **394**, 1595–1605 (2013).

59. Krishnan, K. *et al.* MeCP2 regulates the timing of critical period plasticity that shapes functional connectivity in primary visual cortex. *Proc. Natl. Acad. Sci. USA* **112**, E4782–E4791 (2015).
60. Kishi, N. & Macklis, J.D. MECP2 is progressively expressed in post-migratory neurons and is involved in neuronal maturation rather than cell fate decisions. *Mol. Cell. Neurosci.* **27**, 306–321 (2004).
61. Zhang, W., Peterson, M., Beyer, B., Frankel, W.N. & Zhang, Z.W. Loss of MeCP2 from forebrain excitatory neurons leads to cortical hyperexcitation and seizures. *J. Neurosci.* **34**, 2754–2763 (2014).
62. Chao, H.T., Zoghbi, H.Y. & Rosenmund, C. MeCP2 controls excitatory synaptic strength by regulating glutamatergic synapse number. *Neuron* **56**, 58–65 (2007).
63. Dani, V.S. *et al.* Reduced cortical activity due to a shift in the balance between excitation and inhibition in a mouse model of Rett syndrome. *Proc. Natl. Acad. Sci. USA* **102**, 12560–12565 (2005).
64. Vignoli, A. *et al.* Correlations between neurophysiological, behavioral, and cognitive function in Rett syndrome. *Epilepsy Behav.* **17**, 489–496 (2010).
65. Samuelsson, L., Zagoras, T. & Hafström, M. Inherited 15q24 microdeletion syndrome in twins and their father with phenotypic variability. *Eur. J. Med. Genet.* **58**, 111–115 (2015).
66. Silverstein, R.A. & Ekwall, K. Sin3: a flexible regulator of global gene expression and genome stability. *Curr. Genet.* **47**, 1–17 (2005).
67. Paul, L.K. Developmental malformation of the corpus callosum: a review of typical callosal development and examples of developmental disorders with callosal involvement. *J. Neurodev. Disord.* **3**, 3–27 (2011).
68. Guerrini, R. & Dobyns, W.B. Malformations of cortical development: clinical features and genetic causes. *Lancet Neurol.* **13**, 710–726 (2014).
69. Yu, T.W. *et al.* Mutations in *WDR62*, encoding a centrosome-associated protein, cause microcephaly with simplified gyri and abnormal cortical architecture. *Nat. Genet.* **42**, 1015–1020 (2010).
70. Bilgüvar, K. *et al.* Whole-exome sequencing identifies recessive *WDR62* mutations in severe brain malformations. *Nature* **467**, 207–210 (2010).
71. Chen, J.F. *et al.* Microcephaly disease gene *Wdr62* regulates mitotic progression of embryonic neural stem cells and brain size. *Nat. Commun.* **5**, 3885 (2014).
72. Xu, D., Zhang, F., Wang, Y., Sun, Y. & Xu, Z. Microcephaly-associated protein WDR62 regulates neurogenesis through JNK1 in the developing neocortex. *Cell Reports* **6**, 104–116 (2014).
73. Nicholas, A.K. *et al.* WDR62 is associated with the spindle pole and is mutated in human microcephaly. *Nat. Genet.* **42**, 1010–1014 (2010).
74. Huang, T.N. *et al. Tbr1* haploinsufficiency impairs amygdalar axonal projections and results in cognitive abnormality. *Nat. Neurosci.* **17**, 240–247 (2014).
75. Kolk, S.M., Whitman, M.C., Yun, M.E., Shete, P. & Donoghue, M.J. A unique subpopulation of Tbr1-expressing deep layer neurons in the developing cerebral cortex. *Mol. Cell. Neurosci.* **32**, 200–214 (2006).
76. Bedogni, F. *et al.* Tbr1 regulates regional and laminar identity of postmitotic neurons in developing neocortex. *Proc. Natl. Acad. Sci. USA* **107**, 13129–13134 (2010).
77. Palumbo, O. *et al. TBR1* is the candidate gene for intellectual disability in patients with a 2q24.2 interstitial deletion. *Am. J. Med. Genet. A.* **164A**, 828–833 (2014).
78. Deriziotis, P. *et al. De novo TBR1* mutations in sporadic autism disrupt protein functions. *Nat. Commun.* **5**, 4954 (2014).
79. O'Roak, B.J. *et al.* Multiplex targeted sequencing identifies recurrently mutated genes in autism spectrum disorders. *Science* **338**, 1619–1622 (2012).
80. Kolk, S.M. *et al.* Semaphorin 3F is a bifunctional guidance cue for dopaminergic axons and controls their fasciculation, channeling, rostral growth, and intracortical targeting. *J. Neurosci.* **29**, 12542–12557 (2009).
81. McDonel, P., Costello, I. & Hendrich, B. Keeping things quiet: roles of NuRD and Sin3 co-repressor complexes during mammalian development. *Int. J. Biochem. Cell Biol.* **41**, 108–116 (2009).
82. Lin, T. *et al.* p53 induces differentiation of mouse embryonic stem cells by suppressing *Nanog* expression. *Nat. Cell Biol.* **7**, 165–171 (2005).

ONLINE METHODS

Patient recruitment. All individuals except for individuals 7–9 were ascertained during a clinical genetic diagnostic work-up because of unexplained intellectual disability, at one of the involved genetic diagnostic services in Nijmegen, Groningen, Nantes and Southampton. The total pool of recruitment consisted of over 12,000 individuals with unexplained intellectual disability and developmental delay. This number comprises both SNP-based microchromosomal array cases and whole-exome sequencing cases. With regard to the sequencing cases (individuals 5–7, 10 and 11), these all concern cases from diagnostic whole-exome sequencing. Individuals 5, 6, 10 and 11 were diagnosed from ~2,000 cases of intellectual disability and developmental delay in the Nijmegen laboratory, and individual 7 was diagnosed from 250 cases in the Bonn (Germany) laboratory. Thus, altogether, the frequency of single *SIN3A* mutations is approximately 1 in 250–500 for individuals who underwent whole-exome sequencing because of unexplained intellectual disability and developmental delay. Individuals 3 and 4 were recruited from the Decipher database. Individuals 7–9 were ascertained in a collaborative study Bonn-Essen-Munich of 250 individuals with intellectual disability of unknown origin. Inclusion into this study was in agreement with local medical ethics committee approval. Patients were consented by their legal representatives during the genetic consultation.

Genome-wide chromosome microarray analysis. Different microchromosomal array platforms were used. The deletions in individuals 1 and 2 were identified using the Agilent 105K oligo array. The deletions in individuals 3 and 4 were identified on the Agilent 8 × 60k platform (International Standards for Cytogenomic Arrays (ISCA), Oxford Gene Technology (OGT)). CNVs were mapped according to UCSC Genome Browser build February 2009 (hg19).

Whole-exome sequencing. For individuals 5, 6, 10 and 11, a family-based whole-exome sequencing analysis was performed essentially as previously described[79]. Briefly, capture of exons was performed using an Agilent SureSelect XT Human All Exon 50Mb kit. Sequencing was performed using a Life Technologies 5500XL machine or an Illumina HiSeq 2000 instrument. Read mapping and variant calling were performed using LifeScope for the 5500XL data or BWA (mapping) and GATK (calling) for the Illumina data. In patient 7 and his father (patient 8), whole-exome sequencing was performed on an Illumina HiSeq 2500 instrument after enrichment with version 5 of the SureSelect XT Human All Exon 50Mb kit as published previously. *De novo* mutations in patients 5, 6 and 10 and inherited mutations in patients 7–9 and 11–13 were confirmed by Sanger sequencing.

Mice and preparation of brain cryosections. All animal use, care and experimental procedures were performed in accordance with institutional and national ethical guidelines and regulations and with the approval of the Committee for Animal Experiments of the Radboud University (Nijmegen, the Netherlands) under protocol RU-DEC 2011-190/2011-268/2014-059. The day of vaginal plug was considered E0.5, and the day of birth was considered P0. Timed-pregnant mice (normal C57BL/6JolaHSD background from Harlan Laboratories) and pups were killed by means of cervical dislocation or decapitation, respectively. The embryos were dissected in ice-cold Leibovitz medium (L-15, PAA). Alternatively, postnatal mice were euthanized by decapitation, and both embryonic and postnatal brains were quickly removed from their skulls in L-15 medium. For the PCR experiment, brains and brain areas were quickly frozen in liquid nitrogen and stored at −80 °C before RNA was isolated. For immunohistochemistry, brains were fixed by submersion in 4% paraformaldehyde in PBS, pH 7.4, at 4 °C for 1–1.5 h maximum. After a quick wash in PBS, brains were cryoprotected overnight in 30% sucrose in PBS. Then, brains were frozen in M-1 embedding matrix in a plastic cup (Thermo Fisher Scientific) on dry ice and stored at −80 °C. Cryostat sections were cut at 16 µm, mounted on SuperFrost Plus slides (Thermo Fisher Scientific), air-dried and stored desiccated at −20 °C.

RNA isolation and real-time qPCR. Total RNA from the brains from mice of different ages, individual brain areas and mouse neuroblastoma (N2a) cells was extracted with TRI reagent (Sigma-Aldrich), and 1–2 µg of total RNA was used for cDNA synthesis using the RevertAid H-minus first-strand cDNA synthesis kit (Thermo Scientific). A 1:15 dilution of the cDNA pool was used in a 10-µl reaction for qPCR analysis using the Sensifast SYBR no ROX qPCR kit (Bioline) and a Rotor-Gene 6000 real-time analyzer (Qiagen). The qPCR program used was as follows: 2 min at 95 °C followed by 40 cycles of 5 s at 95 °C, 10 s at 60 or 65 °C, and 15 s at 72 °C. The intron-spanning primers used are listed in **Supplementary Table 1**. Peptidyl prolyl isomerase (*Ppia*) and β-actin (*Actb*) were used as reference transcripts. qPCR data were analyzed by using comparative quantification, and the relative *q* values of the genes of interest were calculated by equalizing the lowest C_t value to 1. The normalization factor for the reference genes was determined using the GeNORM program and used to normalize the *q* values. Individual experiments were performed in triplicate with independent mouse brain or brain area RNA pools from mice of various developmental ages derived from three non-related animals.

Plasmid construction. To downregulate the expression of *Sin3a* in cortical regions, two different shRNA oligonucleotides[83] were cloned via BglII and HindIII restriction sites into pSUPER.GFP/Neo (a kind gift of W. Hendriks): shSin3a-ex13 and shSin3a-ex16 (**Supplementary Fig. 4c–g** and **Supplementary Table 1**). These sequences target different regions of *Sin3a*, respectively, exon 13 and exon 16, and were based on the siRNA sequences described earlier[53]. Reporter CMV-YFP-N1 plasmid and scrambled *Sin3a* sequences cloned into pSUPER.GFP/Neo (sc-shSin3a-ex13 and sc-shSin3a-ex16) were used as controls (**Supplementary Fig. 4c–g** and **Supplementary Table 1**).

For construction of a mouse full-length *Sin3a* shRNA-insensitive construct (mSin3a*), total cDNA from P140 mouse brain was used to amplify two DNA fragments, 5′-MmSin3a and 3′-MmSin3a of, respectively, 2,103 bp and 1,843 bp, by PCR using specific primers (MmSin3a-Ampli 5′part and MmSin3a-Ampli 3′part) as described in **Supplementary Table 1**. Primer sequences were based on NCBI reference sequence NM_001110351.1. Both *Sin3a* cDNA fragments were cloned into the BamHI and SalI restriction sites of pGemzf3+ plasmid resulting in 5′-Sin3a_pGEMzf3+ and 3′ Sin3a_pGEMzf3+. 5′-Sin3a_ pGEMzf3+ was cut via EcoRI and ApaLI, and 3′-Sin3a_ pGEMzf3+ was cut via MunI and BamHI. Both 5′-Sin3a_pGEMzf3+ and 3′-Sin3a_pGEMzf3+ fragments were isolated and purified from agarose gel.

A Gblock gene fragment of 1,000 bp was ordered from IDT (NM_001110351.1: 1,858–2,857) containing mutated target sites for both shSin3a-ex13 (GAGCACATCTATCGATGCG) (NM_001110351.1: 1,986–2,004) and shSin3a-ex16 (GTATGGACGAGGTATACAA) (NM_001110351.1: 2,800–2,818) (mutated positions are underlined) (**Supplementary Table 1**). The three fragments 5′-Sin3A_pGEMzf3+ (MunI–BamHI), 3′-Sin3A_pGEMzf3+ (EcoRI–ApaLI) and the Gblock fragment were assembled via Gibson assembly (New England BioLabs) to generate shRNA-insensitive *Sin3a*(full length)-pGEMzf3+. Finally, the EcoRI–SalI shRNA-insensitive *Sin3a* full-length fragment was isolated and cloned into the EcoRI–XhoI restriction sites of the chicken actin (CAg) promoter–containing mammalian expression plasmid pCAB, resulting in mSin3A*-pCAB. The pCAB expression plasmid was derived from pCAB-EGFP (a kind gift of W. Hendriks) by removing the EGFP coding sequence using SmaI and XhoI (**Supplementary Fig. 4g**).

Cell culture and validation. Mouse N2a cells (under passage 20) were cultured in complete MEM (PAA) containing 10% FBS (PAA), and COS-1 cells were cultured in complete DMEM (Gibco) containing 10% FCS; cells were maintained at 37 °C under a 5.5% CO_2 atmosphere. One day before transfection, cells were seeded at 1×10^5 cells per well in 24-well plates. Cells were transfected with either *Sin3a* siRNA[53] using 1.5 µl of Lipofectamine 2000 (Invitrogen) and 33 nmol of siRNA or with *Sin3a* shRNA constructs using 2.0 µg of plasmid DNA and 2 µl of Lipofectamine LTX (Invitrogen) in OptiMEM (Gibco). siRNA- and shRNA-mediated mRNA degradation was allowed for 48 h, and total RNA was extracted as described. To validate the expression and intracellular localization of protein from full-length shRNA-insensitive *Sin3a*, 4×10^5 COS-1 cells were seeded in 12-well plates and transiently transfected with 3.0 µg of plasmid DNA using Lipofectamine LTX. Recombinant protein expression was allowed for 24 h. Both COS-1 and N2a cells were authenticated and screened for mycoplasma contamination monthly. Experiments were performed in triplicate.

Protein isolation and immunoblotting. Cells were scraped in 1 ml of PBS and collected by centrifugation (5 min, 500*g*, 4 °C). Cells were then lysed in

doi:10.1038/ng.3619

RIPA buffer (150 mM NaCl, 1% NP-40, 0.5% SDS, 50 mM Tris-HCl, pH 8.0, 2 mM EDTA and Complete protease inhibitors (Roche)) and sonicated. Equal amounts of cell lysates were separated by 7% SDS–PAGE and subsequently transferred to a PVDF membrane (Bio-Rad). The membrane was incubated with an antibody against Sin3a (1:2,000 dilution; Abcam) and secondary peroxidase-conjugated goat-anti-rabbit antibody (1:5,000 dilution; Nordic) followed by chemoluminescence (LumiLight Plus, Roche). Signals were detected using the LAS4000 imaging system (GE Healthcare). Experiments were performed in triplicate.

***In utero* electroporation.** *In utero* electroporation was performed as described previously with minor modifications[29,84]. Briefly, timed-pregnant (E14.5) mice were anaesthetized with a 100 mg/kg ketamine and 10 mg/kg xylazine cocktail. After laparotomy, a solution containing plasmid DNA (2 μg/μl CMV-YFP-N1 or 2 μg/μl shSin3a-ex13, shSin3a-ex16, sc-shSin3a-ex16, or shSin3a-ex13 + 2 μg/μl or 4 μg/μl mSin3a* in Tris-buffered 0.02% Fast Green) was injected through the uterine wall into the lateral ventricle of each embryo using calibrated pulled-glass capillaries (WPI) and a microinjector (BTX Microject 1000, Harvard Apparatus). A series of five unipolar square-wave current pulses (33 V max) from an electroporator (ECM 830, BTX, Harvard Apparatus) was delivered over each embryo's head using tweezers-type electrodes (BTX). Embryos were kept hydrated during the procedure and placed back into the abdomen of the mother; gestation was allowed to proceed for 3 d. Only embryos showing effective transfection in the somatosensory cortex were included for analysis, and brains were processed for cryosectioning as described earlier.

Immunofluorescent staining and fluorescent microscopy. Cryosections were rehydrated in PBS (0.08 M Na_2HPO_4, 1.36 M NaCl, 0.017 M KH_2PO_4 and 0.026 M KCl). Sections were incubated in normal blocking solution (1.3% normal goat serum, 1.3% normal donkey serum, 1.3% normal horse serum, 1% BSA, 0.1% glycine, 0.1% lysine and 0.4% Triton X-100; NBS) for 1 h at room temperature. Primary antibodies, which are listed in **Supplementary Table 2**, diluted in NBS were incubated with sections overnight at 4 °C. Slides were washed three times in PBS for a total of 30 min at room temperature. Species-specific Alexa Fluor–conjugated secondary antibodies (Molecular Probes) diluted in NBS were incubated with sections for 1 h at room temperature. After three washes in PBS for a total of 30 min at room temperature, sections were incubated with blue fluorescent Nissl stain (1:500 dilution; NeuroTrace, Invitrogen) for 15 min and washed four times in PBS, 10 min each wash, at room temperature. Slides were mounted in 90% glycerol in PBS. Staining was visualized and images were captured using a Leica DMRA fluorescence microscope coupled with a DFC340FX digital camera and LASAF software.

For immunofluorescent staining of transfected COS-1 cells, cells were cultured on coverslips, and 24 h after transfection cells were washed twice with PBS and fixed with 4% paraformaldehyde in PBS for 1 h at 4 °C. Next, cells were washed with 50 mM NH_4Cl in PBS and permeabilized with 0.1% Triton X-100 in PBS (PBS-T). Subsequently, cells were incubated with the antibody to Sin3a (1:500 dilution) in blocking buffer (PBS-T and 1% BSA) for 16 h at 4 °C. After PBS-T washing steps, cells were incubated for 1 h at room temperature with secondary antibody (Alexa Fluor 488–conjugated goat anti-rabbit antibody (Molecular Probes; 1:200 dilution) in blocking buffer. Finally, cells were washed with PBS-T, PBS and MilliQ water, dehydrated with methanol, air-dried and embedded in Mowiol. Microscopic imaging was performed using an Olympus FV1000 laser scanning microscope.

Cell proliferation analysis. Pregnant mothers with electroporated embryos received an intraperitoneal injection of 5-bromo-2′-deoxyuridine (BrdU; BD Biosciences; 50 μg/g) 1.5 h before euthanasia to label cells in S phase before they enter mitosis. Embryonic brains were quickly dissected, fixed, frozen and sectioned. Cryosections were incubated with NBS for 1 h at room temperature and then incubated with chicken antibody to GFP and rabbit antibody to Ki-67 diluted in NBS overnight at 4 °C as described[29]. Cryosections were postfixed for 10 min in 4% paraformaldehyde, followed by a quick wash step in PBS. Subsequently, sections were treated with 0.1% trypsin in 0.1% $CaCl_2$ in 0.1 M Tris for 10–15 s, incubated in 100% FBS or FCS for 10 min and rinsed in PBS. Sections were incubated in 2 N HCl for 30 min at 37 °C with agitation, the acid was neutralized in 0.1 M sodium borate, pH 8.5, and sections were quickly washed in PBS. Standard immunohistochemistry using chicken antibody to GFP, rabbit antibody to Ki-67 (**Supplementary Table 2**) and mouse antibody to BrdU was then performed as described above. To calculate the rate of proliferation of the transfected cells, the number of double-positive cells was determined in the proliferating zone.

Data analyses. To assess the number of GFP^+ neurons in the electroporated area, 2–7 embryos or pups were analyzed and 2–5 well-spaced (128 μm) sections at the same neuroanatomical level were imaged for each embryo as described[80] . A 0.15-mm-wide rectangle spanning the cerebral wall was placed over the center of the transfected area in the somatosensory cortex. The cortical swatch was divided into three zones in this rectangle—the proliferative zone (including the ventricular zone and subventricular zone), the intermediate zone and the cortical plate—which were identified on the basis of cell density and polarity visualized by fluorescent Nissl. GFP^+ cells, marker-positive cells and total cells stained by fluorescent Nissl were counted using ImageJ software (NIH) and Adobe Photoshop software. GFP^+ double- or triple-positive cells were quantified in the same way. Data were either normalized to the total number of GFP^+ or $GFP^+Ki\text{-}67^+$ cells or to surface area. All cell number quantifications were performed with blinding and were carried out by two independent individual researchers (J.S.W. and T.C.D.D.). For quantification of neurite growth, three bins of equal size (50 μm) were drawn along the axon bundle 50 μm apart, and the average number of neurites in each bin was determined. The total length of each bundle was determined by tracking the 20 longest neurites using NeuronJ (ImageJ plugin). Data were statistically analyzed by one-way ANOVA analysis of variance ($\alpha = 5\%$) using GraphPad Prism software and are expressed as means ± s.e.m. Differences between groups were considered significant for $P < 0.05$.

83. Yuan, B., Latek, R., Hossbach, M., Tuschl, T. & Lewitter, F. siRNA Selection Server: an automated siRNA oligonucleotide prediction server. *Nucleic Acids Res.* **32**, W130–W134 (2004).
84. North, H.A. *et al.* Promotion of proliferation in the developing cerebral cortex by EphA4 forward signaling. *Development* **136**, 2467–2476 (2009).